INTERNATIONAL JOURNAL FOR NUMERICAL METHODS IN FLUIDS
Int. J. Numer. Meth. Fluids 2008; **58**:1063–1080
Published online 1 April 2008 in Wiley InterScience (www.interscience.wiley.com). DOI: 10.1002/fld.1771

Effect of blockage on free vibration of a circular cylinder at low *Re*

T. K. Prasanth and S. Mittal*, †

Department of Aerospace Engineering, Indian Institute of Technology, Kanpur, UP 208 016, India

SUMMARY

The effect of the blockage on vortex-induced vibrations of a circular cylinder of low non-dimensional mass ($m^* = 10$) in the laminar flow regime is investigated in detail. A stabilized space–time finite element formulation is utilized to solve the incompressible flow equations in primitive variables form in two dimensions. The transverse response of the cylinder is found to be hysteretic at both ends of synchronization/lock-in region for 5% blockage. However, for the 1% blockage hysteresis occurs only at the higher *Re* end of synchronization/lock-in region. Computations are carried out at other blockages to understand its effect on the hysteretic behavior. The hysteresis loop at the lower *Re* end of the synchronization decreases with decrease in blockage and is completely eliminated for blockage of 2.5% and less. On the other hand, hysteresis persists for all values of blockage at the higher *Re* end of synchronization/lock-in. Although the peak transverse oscillation amplitude is found to be same for all blockage ($\sim 0.6D$), the peak value of the aerodynamic coefficients vary significantly with blockage. The r.m.s. values show lesser variation with blockage. The effect of streamwise extent of computational domain on hysteretic behavior is also studied. The phase between the lift force and transverse displacement shows a jump of almost 180° at, approximately, the middle of the synchronization region. This jump is not hysteretic and is independent of blockage. Copyright © 2008 John Wiley & Sons, Ltd.

Received 14 October 2007; Revised 22 December 2007; Accepted 2 January 2008

KEY WORDS: circular cylinder; hysteresis; synchronization; lock-in; blockage effect; phase jump; free vibrations; vortex-induced vibrations

1. INTRODUCTION

The problem of vortex-induced vibration (VIV) is of importance in several engineering applications because of the large amplitude of oscillations and significant changes in unsteady forces compared with those encountered for flow past stationary bodies. VIV is associated with various interesting phenomena. One of them is the synchronization/lock-in of the vortex-shedding frequency to the oscillation frequency of the body over a range of Reynolds numbers. Another interesting

*Correspondence to: S. Mittal, Department of Aerospace Engineering, Indian Institute of Technology, Kanpur, UP 208 016, India.
†E-mail: smittal@iitk.ac.in

phenomenon is the hysteresis in the response of the cylinder and the flow. Based on the response of the cylinder and modes of vortex shedding the synchronization region has been classified into various *branches*. For a comprehensive review of the research on various aspects of VIVs, the reader is referred to the review articles by Williamson and Govardhan [1], Bearman [2] and Sarpkaya [3, 4].

Synchronization and hysteresis were observed in free and forced vibration studies by Feng [5] and Bishop and Hassan [6] and by many researchers thereafter. Synchronization/lock-in is accompanied with jumps in transverse vibration amplitude (A/D) and fluid forces on the body. In addition, the phase difference between the cylinder displacement and fluid forces also shows a sharp change. Khalak and Williamson [7] conducted experiments involving transverse oscillations of an elastically mounted rigid cylinder at very low mass damping, $m^*\zeta$. They showed that depending on the value of the combined mass-damping parameter the response of the cylinder can be one of the two types. For low $m^*\zeta$ the response consists of three branches: initial excitation, upper and lower. The transition between the initial and upper branches involves hysteresis. Intermittent switching of flow modes is observed for the transition between the upper and lower branches. For high $m^*\zeta$ only two response branches are seen. This is often referred to as the classical Feng-type response. Brika and Laneville [8] in their experimental investigation of VIV of a long flexible circular cylinder with low damping ratio observed hysteresis in the transverse displacement of the cylinder with variation of flow velocity. Two branches of cylinder response were reported depending on whether flow velocity is varied gradually or impulsively.

Although hysteresis has been reported by many researchers in the higher *Re* regime [7, 8], it was discovered in the laminar regime not too long ago. Williamson and Govardhan [1] demonstrated, via compilation of results from the literature for various studies, that hysteresis at the low velocity end of synchronization region may exist even in the laminar vortex-shedding range. Singh and Mittal [9] also found hysteresis via their numerical simulations. They showed for the first time that in the laminar flow regime the hysteresis also exists near the higher *Re* end of the lock-in regime. They also showed that the hysteretic behavior persists even when the cylinder is allowed to oscillate only in transverse direction. Recently, Klamo *et al.* [10] also reported hysteresis at the higher U^* end of synchronization/lock-in. The cause of the hysteretic behavior is usually attributed to sudden change in the wake modes [8, 11].

The variation of phase (ϕ), between the transverse displacement and lift force, is found to undergo a sudden jump in forced vibration studies. This was first reported by Bishop and Hassan [6]. Ongoren and Rockwell [12, 13], in their forced vibration experiments, have observed a phase shift of $\sim 180^\circ$ when the frequency ratio f_e/f_0 was increased through unity. Here f_e is the excitation frequency and f_0 is the natural shedding frequency. During this transition, a switch in the phase of initially shed vortex to the opposite side of the cylinder is observed. Khalak and Williamson [7] and Govardhan and Williamson [14], in their study of VIVs at low mass damping, observed that the 180° jump in phase angle takes place only when the flow jumps between upper–lower branches of response.

Even though a blockage of 5% is sufficient for computing flow past a stationary cylinder, it may not be sufficient for computations of flow past a vibrating cylinder because of the much wider wake in the later case [15]. Barring the study of Brika and Laneville [8], the blockage for the investigations discussed above is larger than 5%. For example, it is 8.3% for Feng [5], 8.4% for Bishop and Hassan [6], 4.2 and 8.3% for Carberry *et al.* [16] and 10% for Khalak and Williamson [7]. More details on the blockage used for various experimental studies can be found in the compilation by Norberg [17] and Williamson and Govardhan [1]. The blockage for the

DOI: 10.1002/fld

numerical investigations by Singh and Mittal [9] is 5%. It is 6.25% for the study by Mittal and Tezduyar [18]. Stansby [19] in his forced oscillation study observed hysteresis in the jump in phase ϕ between the component of hot wire signal at cylinder frequency and the cylinder displacement. However, the hysteresis was observed only for a cylinder with larger diameter corresponding to 7.2% blockage. The cylinder with smaller diameter, leading to 3.6% blockage, did not exhibit a hysteretic behavior in phase jump. This was attributed to the blockage effect.

Most of the VIV experiments in the past have been carried out at *Re* beyond the laminar regime. It is well known that there are differences in the hysteretic response of cylinder undergoing VIV at higher *Re* compared with that in the laminar regime ($Re<200$). In this paper, we investigate the effect of blockage on the hysteretic behavior of the cylinder at low *Re* in the laminar flow regime. We also study the effect of blockage on the variation of phase between the transverse displacement and lift force. The effect of blockage from the present study are not necessarily relevant at higher *Re*. The computations at higher *Re* need to be carried out in three dimensions and are expected to be significantly more expensive.

2. THE GOVERNING EQUATIONS

2.1. The incompressible flow equations

Let $\Omega_t \subset \mathbb{R}^{n_{sd}}$ and $(0, T)$ be the spatial and temporal domains, respectively, where n_{sd} is the number of space dimensions, and let Γ_t denote the boundary of Ω_t. The spatial and temporal coordinates are denoted by $\mathbf{x}$ and t. The Navier–Stokes equations governing incompressible fluid flow are

$$\rho\left(\frac{\partial \mathbf{u}}{\partial t}+\mathbf{u}\cdot\nabla\mathbf{u}-\mathbf{f}\right)-\nabla\cdot\boldsymbol{\sigma}=0 \quad \text{on } \Omega_t\times(0,T) \tag{1}$$

$$\nabla\cdot\mathbf{u}=0 \quad \text{on } \Omega_t\times(0,T) \tag{2}$$

Here ρ, $\mathbf{u}$, $\mathbf{f}$ and $\boldsymbol{\sigma}$ are the density, velocity, body force and the stress tensor, respectively. The stress tensor is expressed as the sum of its isotropic and deviatoric parts:

$$\boldsymbol{\sigma}=-p\mathbf{I}+\mathbf{T}, \quad \mathbf{T}=2\mu\boldsymbol{\varepsilon}(\mathbf{u}), \quad \boldsymbol{\varepsilon}(\mathbf{u})=\tfrac{1}{2}((\nabla\mathbf{u})+(\nabla\mathbf{u})^{\mathrm{T}}) \tag{3}$$

where p and μ are the pressure and dynamic viscosity, respectively. Both Dirichlet- and Neumann-type boundary conditions are accounted for and are represented as

$$\mathbf{u}=\mathbf{g} \quad \text{on } (\Gamma_t)_g, \quad \mathsf{n}\cdot\boldsymbol{\sigma}=\mathbf{h} \quad \text{on } (\Gamma_t)_h \tag{4}$$

where $(\Gamma_t)_g$ and $(\Gamma_t)_h$ are complementary subsets of the boundary Γ_t and n is its unit normal vector. More details on the boundary conditions are shown in Figure 1 and described later in Section 4. The initial condition on the velocity is specified on Ω_t at $t=0$:

$$\mathbf{u}(\mathbf{x},0)=\mathbf{u}_0 \quad \text{on } \Omega_0 \tag{5}$$

where $\mathbf{u}_0$ is divergence free.

DOI: 10.1002/fld

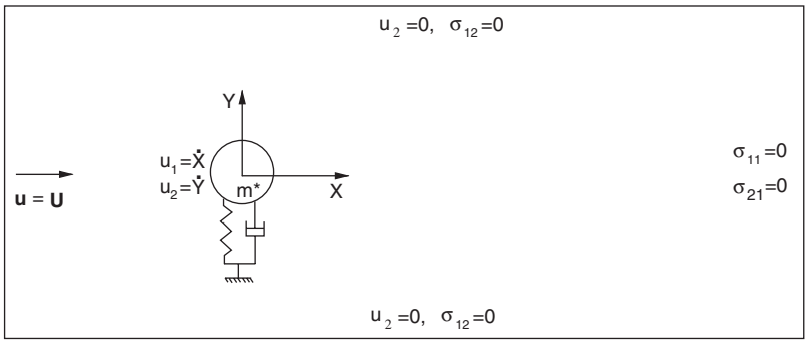

Figure 1. Vortex-induced vibrations of a cylinder: schematic of the problem setup. The boundary conditions are also shown in the figure.

2.2. *The equations of motion for a rigid body*

A solid body immersed in the fluid experiences unsteady forces and in certain cases may exhibit rigid body motion. The motion of the body, in the two directions along the Cartesian axes, is governed by the following equations:

$$\ddot{X}+4\pi F_{\mathrm{N}}\zeta\dot{X}+(2\pi F_{\mathrm{N}})^2X=\frac{2C_{\mathrm{D}}}{\pi m^*} \quad \text{for } (0,T) \tag{6}$$

$$\ddot{Y}+4\pi F_{\mathrm{N}}\zeta\dot{Y}+(2\pi F_{\mathrm{N}})^2Y=\frac{2C_{\mathrm{L}}}{\pi m^*} \quad \text{for } (0,T) \tag{7}$$

Here, F_{N} is the reduced natural frequency of the oscillator, ζ the structural damping ratio, m^* the non-dimensional mass of the body, and C_{L} and C_{D} are the instantaneous lift and drag coefficients for the body, respectively. The free-stream flow is assumed to be along the x-axis. $\ddot{X}$, $\dot{X}$ and X denote the normalized in-line acceleration, velocity and displacement of the body, respectively, while $\ddot{Y}$, $\dot{Y}$ and Y represent the same quantities associated with the cross-flow motion. In the present study, in which the rigid body is a circular cylinder, the displacement and velocity are normalized by the diameter, D, of the cylinder and the free-stream speed, U, respectively. The reduced natural frequency of the system, F_{N} is defined as $f_{\mathrm{N}}D/U$ where f_{N} is the natural frequency of the oscillator. Another related parameter is the reduced velocity, U^*. It is defined as $U^*=U/f_{\mathrm{N}}D=1/F_{\mathrm{N}}$.

The non-dimensional mass of the cylinder is defined as $m^*=4m/\pi\rho D^2$ where m is the actual mass of the oscillator per unit length and ρ is the density of the fluid. The force coefficients are computed by carrying an integration that involves the pressure and viscous stresses around the circumference of the cylinder.

3. THE FINITE ELEMENT FORMULATION

To accommodate the motion of the cylinder and the deformation of the mesh, a formulation that can handle moving boundaries and interfaces is employed. In order to construct the finite element function spaces for the space–time method, we partition the time interval $(0,T)$ into

DOI: 10.1002/fld

subintervals $I_n=(t_n,t_{n+1})$, where t_n and t_{n+1} belong to an ordered series of time levels: $0=t_0<t_1<\cdots<t_N=T$. Let $\Omega_n=\Omega_{t_n}$ and $\Gamma_n=\Gamma_{t_n}$. We define the space–time slab Q_n as the domain enclosed by the surfaces Ω_n, Ω_{n+1}, and P_n, where P_n is the surface described by the boundary Γ_t as t traverses I_n. As is the case with Γ_t, the surface P_n is decomposed into $(P_n)_g$ and $(P_n)_h$ with respect to the type of boundary condition (Dirichlet or Neumann) being imposed. For each space–time slab we define the corresponding finite element function spaces: $(\mathscr{S}^h_{\mathbf{u}})_n$, $(\mathscr{V}^h_{\mathbf{u}})_n$, $(\mathscr{S}^h_p)_n$ and $(\mathscr{V}^h_p)_n$. Over the element domain, this space is formed by using first-order polynomials in space and time. Globally, the interpolation functions are continuous in space but discontinuous in time.

The stabilized space–time formulation for deforming domains is then expressed as follows: given $(\mathbf{u}^h)_{n^-}$, find $\mathbf{u}^h\in(\mathscr{S}^h_{\mathbf{u}})_n$ and $p^h\in(\mathscr{S}^h_p)_n$ such that $\forall\mathbf{w}^h\in(\mathscr{V}^h_{\mathbf{u}})_n$, $q^h\in(\mathscr{V}^h_p)_n$,

$$\begin{aligned}
&\int_{Q_n}\mathbf{w}^h\cdot\rho\left(\frac{\partial\mathbf{u}^h}{\partial t}+\mathbf{u}^h\cdot\nabla\mathbf{u}^h-\mathbf{f}\right)\mathrm{d}\Omega+\int_{Q_n}\boldsymbol{\varepsilon}(\mathbf{w}^h):\boldsymbol{\sigma}(p^h,\mathbf{u}^h)\,\mathrm{d}Q+\int_{Q_n}q^h\nabla\cdot\mathbf{u}^h\,\mathrm{d}Q\\
&\quad+\sum_{e=1}^{n_{el}}\int_{Q_n^e}\frac{1}{\rho}\tau\left[\rho\left(\frac{\partial\mathbf{w}^h}{\partial t}+\mathbf{u}^h\cdot\nabla\mathbf{w}^h\right)-\nabla\cdot\boldsymbol{\sigma}(q^h,\mathbf{w}^h)\right]\\
&\quad\cdot\left[\rho\left(\frac{\partial\mathbf{u}^h}{\partial t}+\mathbf{u}^h\cdot\nabla\mathbf{u}^h-\mathbf{f}\right)-\nabla\cdot\boldsymbol{\sigma}(p^h,\mathbf{u}^h)\right]\mathrm{d}Q\\
&\quad+\sum_{e=1}^{n_{el}}\int_{Q_n^e}\delta\nabla\cdot\mathbf{w}^h\rho\nabla\cdot\mathbf{u}^h\,\mathrm{d}Q+\int_{\Omega_n}(\mathbf{w}^h)_n^+\cdot\rho\left((\mathbf{u}^h)_n^+-(\mathbf{u}^h)_n^-\right)\mathrm{d}\Omega=\int_{(P_n)_h}\mathbf{w}^h\cdot\mathbf{h}^h\,\mathrm{d}P
\end{aligned}\tag{8}$$

This process is applied sequentially to all the space–time slabs $Q_0, Q_1, \ldots, Q_{N-1}$. In the variational formulation given by Equation (8), the following notation is being used:

$$(\mathbf{u}^h)_n^{\pm}=\lim_{\varepsilon\to0}\mathbf{u}(t_n\pm\varepsilon)\tag{9}$$

$$\int_{Q_n}(\cdots)\,\mathrm{d}Q=\int_{I_n}\int_{\Omega_n}(\cdots)\,\mathrm{d}\Omega\,\mathrm{d}t\tag{10}$$

$$\int_{P_n}(\cdots)\,\mathrm{d}P=\int_{I_n}\int_{\Gamma_n}(\cdots)\,\mathrm{d}\Gamma\,\mathrm{d}t\tag{11}$$

The computations start with

$$(\mathbf{u}^h)_0^-=\mathbf{u}_0\tag{12}$$

where $\mathbf{u}_0$ is divergence free.

The variational formulation given by Equation (8) includes certain stabilization terms added to the basic Galerkin formulation to enhance its numerical stability. Details on the formulation, including the definitions of the coefficients τ and δ, can be found in the papers by Tezduyar *et al.* [20–22]. The equations of motion for the oscillator given by Equation (6)–(7) are also cast in the space–time formulation in the same manner as described in the work by Tezduyar *et al.* [22].

DOI: 10.1002/fld

4. PROBLEM DESCRIPTION

A schematic of the problem setup is shown in Figure 1. The cylinder is mounted on elastic supports and is free to undergo oscillations in both transverse as well as streamwise directions. The non-dimensional mass of the cylinder is $m^* = 10.0$. To encourage high amplitude oscillations, the structural damping coefficient is set to zero. It is assumed that the spring mass system is associated with a dimensional natural frequency that does not vary with Reynolds number. As a result, $U^* = U/f\,D$ varies with Re. Here, Re is based on the free-stream speed (U), diameter of the cylinder (D) and viscosity of the fluid. The springs in, both, the transverse and in-line directions are assumed to be identical and exhibit linear behavior. The mass of the oscillator and the spring stiffness are chosen such that the non-dimensional natural frequency matches the vortex-shedding frequency of a stationary cylinder at $Re = 100$, approximately. For all the studies presented in this paper, the variation of the non-dimensional natural frequency with Reynolds number is given as $F_N = 16.6/Re$.

4.1. Boundary conditions

The details of the boundary conditions are shown in Figure 1. No-slip condition is applied to the velocity at the cylinder surface. The location of the cylinder and the flow velocity on its surface are updated at each non-linear iteration of the solution to the flow equations. Free-stream values are assigned for the velocity at the upstream boundary and the viscous stress vector is set to zero at the downstream boundary. On the upper and lower boundaries, the component of the velocity normal to and the component of the stress vector along the boundaries are prescribed zero value.

4.2. Finite element mesh and mesh-moving scheme

The cylinder resides in a rectangular computational domain whose upstream and downstream boundaries are located at distances L_u and L_d, respectively, from the center of the cylinder. The lateral boundaries are separated by a distance H. Figure 2 shows a typical finite element mesh used

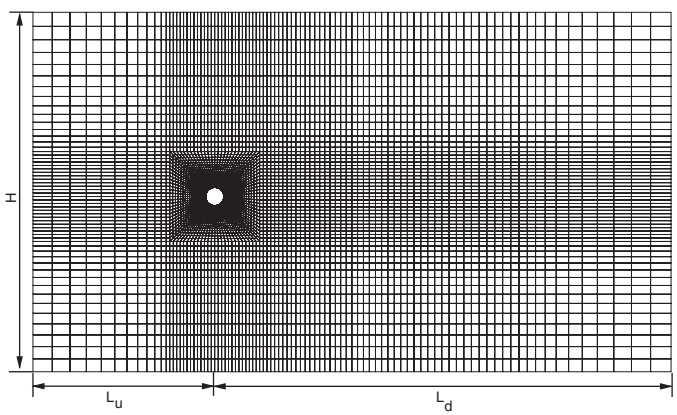

Figure 2. A typical finite element mesh with 7437 nodes and 7236 elements. The location of various boundaries are also shown.

DOI: 10.1002/fld

for the computations. The blockage ratio, B, is defined as $B = D/H$. For the mesh shown in Figure 2, B is 5%. The mesh-moving scheme has been designed such that the mesh in the square box around the cylinder moves along with it as a rigid body. The location of the outer boundary is fixed. As a result, the movement of the cylinder causes deformation of the mesh points lying between the square region and the outer boundary. This kind of mesh movement is expected to lead to almost no projection errors in the flow close to the cylinder. This scheme has been used in our earlier work; for example, in Mittal and Kumar [23] for single cylinder and in Mittal and Kumar [24] for a pair of cylinders.

5. RESULTS

In the present study, computations are carried out for blockages varying from 1 to 5% for a range of Reynolds numbers ($60 \leqslant Re \leqslant 150$) in the laminar regime. A detailed study of mesh resolution and effect of time step on convergence of results can be found in Prasanth *et al.* [15] and Prasanth and Mittal [25]. Two sets of computations are carried out for each blockage. Points on the *increasing branch* are computed by progressively increasing the Reynolds number in small steps. The solution at a lower *Re* is used as the initial condition for the next higher *Re*. Similarly, the *decreasing branch* is traced by progressively decreasing the Reynolds number. Here, the solution at a higher *Re* is used as the initial condition for the next lower *Re*.

5.1. Overview of results

Figures 3 and 4 show an overview of the variation of the response of cylinder and aerodynamic coefficients with *Re* for (a) a high blockage of 5%, (b) an intermediate blockage of 2.5% and (c) a very low blockage of 1%. The left column in Figure 3 shows the variation of maximum transverse oscillation amplitude with *Re* for blockages 5, 2.5 and 1%. Synchronization/lock-in is observed for a range of *Re* (and U^*) at all blockages. Lock-in is associated with large amplitude oscillations of the cylinder. The peak amplitude of the transverse vibrations is $\sim 0.6D$. The response of the cylinder for *increasing* and *decreasing branches* is virtually the same everywhere except near the onset and termination of synchronization. Hysteresis, with respect to increasing *vs* decreasing *Re*, is observed on both low and high *Re* ends of lock-in for 5% blockage (Figure 3(a)). The hysteresis loop width near the higher *Re* end of lock-in is much larger (~ 5 times) when compared with that near the lower *Re* end. Interestingly at lower blockages of 2.5 and 1% the hysteretic behavior near the lower *Re* end of lock-in is not observed. On the contrary, the cylinder response at the higher *Re* end of lock-in is hysteretic irrespective of the blockage. The right column of Figure 3 shows the variation of r.m.s. value of in-line oscillation of the cylinder with *Re* at various blockages. The in-line response amplitude is much smaller than the transverse response. For lower blockage the hysteresis in the in-line response of the cylinder, at the lower *Re* range of lock-in, is replaced by a sharp increase in the in-line oscillations.

Figure 4 shows the variation of lift coefficient and non-dimensionalized vortex-shedding frequency with *Re* for various blockages. The variation of lift coefficient and vortex-shedding frequency are a reflection of changes in the flow pattern. At high blockage (5%) the lift coefficient also shows hysteretic behavior at both ends of lock-in (Figure 4(a)). The maximum value of lift coefficient is observed near the lower *Re* end of lock-in. After reaching the peak, it decreases with

DOI: 10.1002/fld

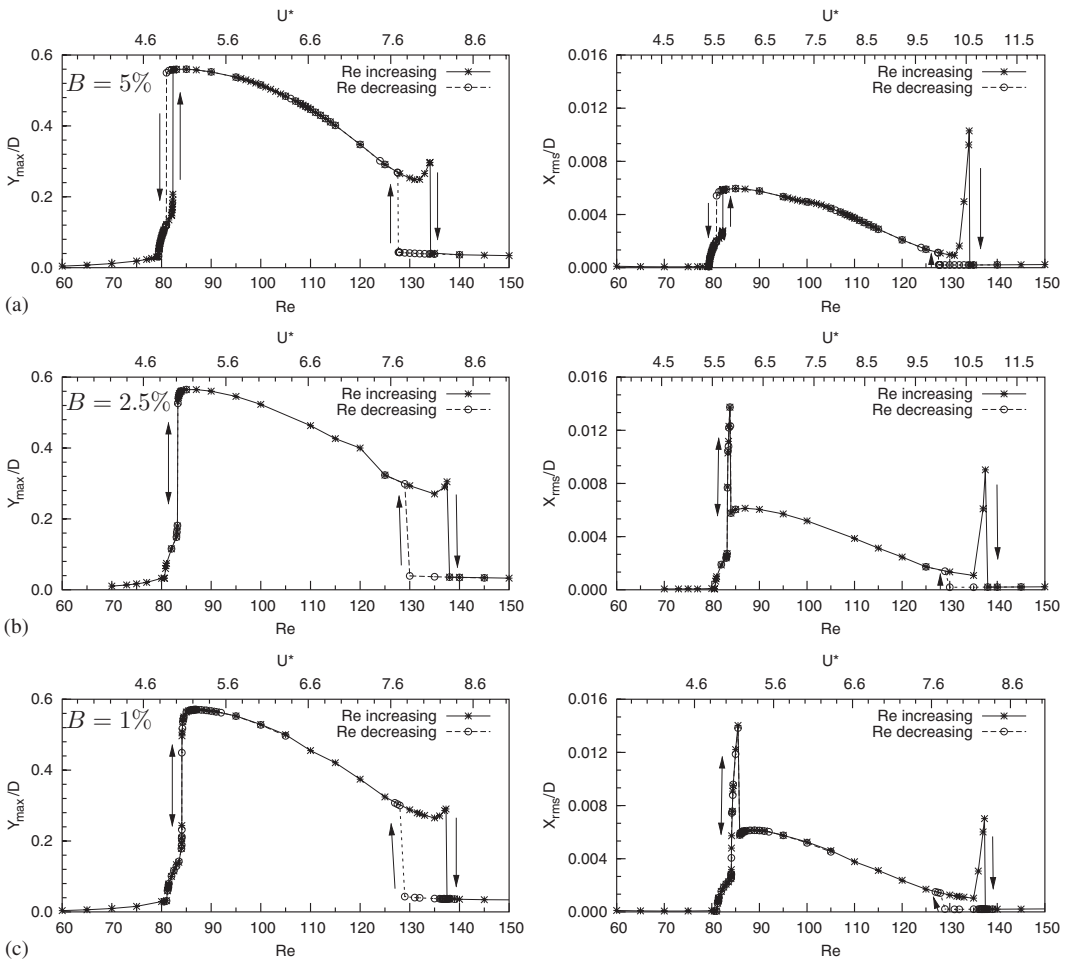

Figure 3. Variation of maximum transverse displacement (left) and *r.m.s* value of in-line displacement (right) with *Re* for various blockages: (a) $B = 5\%$; (b) $B = 2.5\%$; and (c) $B = 1\%$.

increase in *Re*. During the second-half of lock-in region ($Re > 110$), the value of lift coefficient is very low, lower than that of a stationary cylinder. Similar to the cylinder response, the lift coefficient also shows a non-hysteretic behavior near the lower *Re* end of lock-in at lower blockages (2.5 and 1%). Interestingly, the peak value of lift coefficient is very high at lower blockages compared with that at higher blockage.

Synchronization/lock-in for a range of *Re* is evident from the variation of vortex-shedding frequency shown in the right column of Figure 4. During synchronization, the vortex-shedding frequency is significantly different from that of a stationary cylinder. It changes very sharply at the onset of lock-in and achieves a value that is close to the natural frequency of the system. It has been shown in the past (for example, [1]) that at lock-in the vortex-shedding frequency need not be the same as the natural frequency of the oscillator. At the lower *Re* end of the lock-in,

DOI: 10.1002/fld

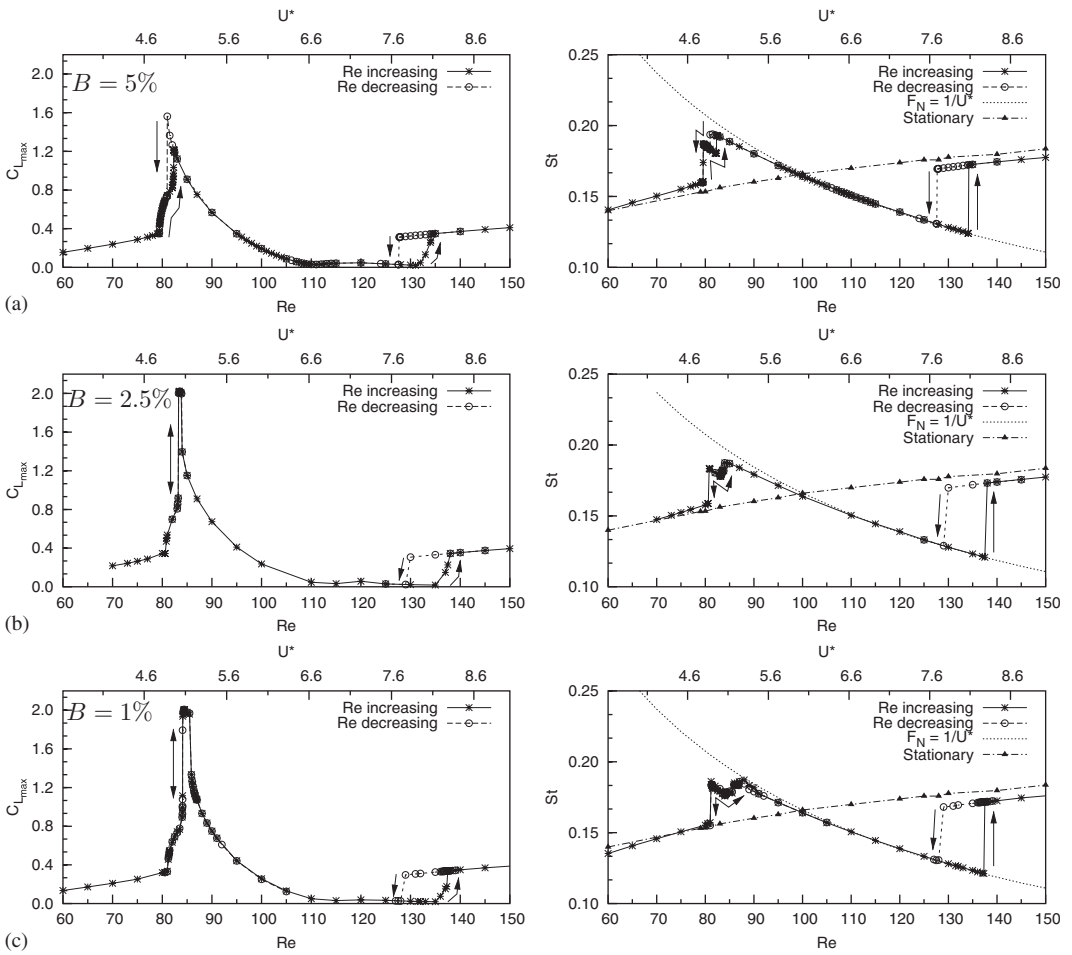

Figure 4. Variation of maximum lift coefficient (left) and non-dimensionalized vortex-shedding frequency (right) with *Re* for various blockages: (a) $B = 5\%$; (b) $B = 2.5\%$; and (c) $B = 1\%$.

the jump in the vortex-shedding frequency seems to occur in two stages. In the first stage, the vortex-shedding frequency jumps to a value that is somewhere in between the natural frequency and the vortex-shedding frequency for the stationary cylinder. This jump is followed by a lock-in-like behavior in the sense that the vortex shedding and cylinder vibration are identical. In the second stage, the lock-in frequency jumps to a value very close to the natural frequency of the system. The jump in the first stage is found to be non-hysteretic at all blockages. The second jump is hysteretic at 5% blockage, whereas it is not hysteretic at lower blockages of 2.5% and less. At the higher *Re* end the hysteretic behavior persists at all blockages. Interestingly, the vibrations of the cylinder has some effect on vortex-shedding frequency beyond the lock-in region also. This can be seen from the slight departure of the two curves for vortex shedding for the vibrating and stationary cylinder, especially at higher *Re*.

DOI: 10.1002/fld

5.2. *Vortex-shedding modes at the onset of synchronization/lock-in*

The synchronization/lock-in is associated with sudden change in vortex-shedding modes. This is reflected in the variation of shedding frequency and the aerodynamic coefficients as seen in Figure 4. Since the maximum amplitude of transverse oscillation possible for VIV in the laminar regime is limited to $\sim 0.6D$, the only possible vortex-shedding modes are $2S$ and $C(2S)$ [11]. In the $2S$ mode of shedding, a single vortex is shed alternately from each side of the cylinder during a vortex-shedding cycle. The $C(2S)$ mode of vortex shedding is similar to the $2S$ mode, but the vortices coalesce in the wake downstream of the cylinder. The $2S$ mode of vortex shedding is associated with low amplitude response in the transverse direction. The $C(2S)$ mode of vortex shedding corresponds to large amplitude of transverse response of the cylinder.

At each blockage studied, two branches of response, the *increasing* and *decreasing* branches, have been computed. The computations, at each Re, are carried out for 500 cycles of vortex shedding, approximately. If the response is hysteretic in nature, it is possible to have both lower as well as large amplitude of transverse oscillation at a Reynolds number depending on whether one is looking at the *increasing* or *decreasing* branch. We demonstrate this by looking at the cylinder response and flow at $Re = 81.5$. Figure 5 shows the time histories of transverse oscillation of the cylinder and lift coefficient at Reynolds number, $Re = 81.5$, for a blockage of 5%. The left column shows the response of the cylinder at $Re = 81.5$ for the *increasing Re* branch, whereas the right column shows the response of the cylinder at $Re = 81.5$ for the *decreasing Re* branch. The corresponding vorticity fields are also shown for both cases. A low amplitude response is observed for the *increasing Re* branch where the time histories display a 'beating' behavior.

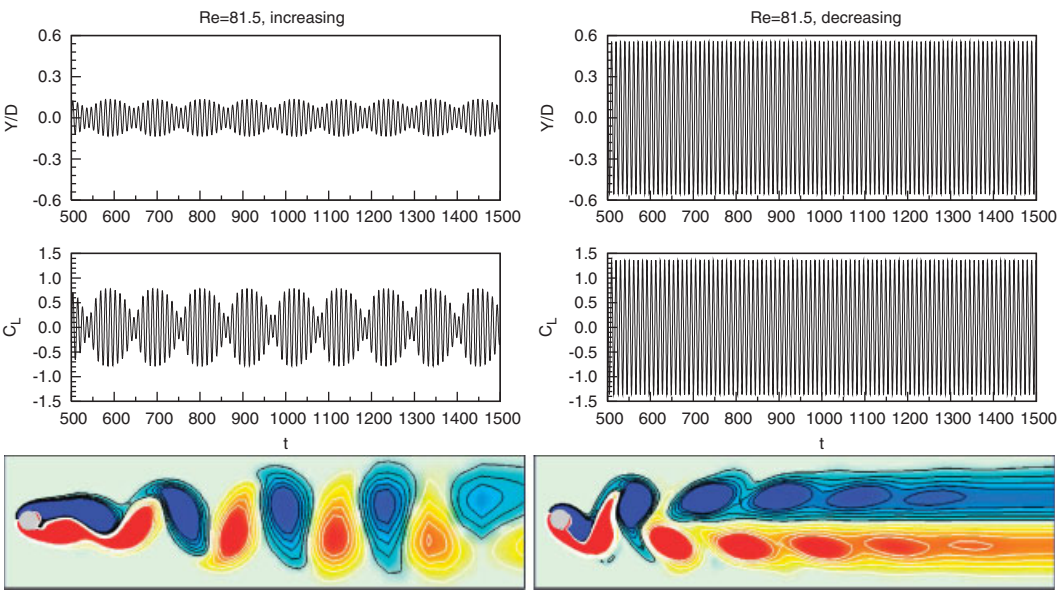

Figure 5. $Re = 81.5$, $B = 5\%$ flow past a freely vibrating cylinder: time histories of the lift coefficient and transverse oscillation of the cylinder for, both, increasing and decreasing branches. Also shown is the vorticity field for the fully developed unsteady flow for the two cases.

DOI: 10.1002/fld

The vortex-shedding mode observed is $2S$ for this case. On the other hand, for the *decreasing Re* branch, large amplitude of oscillation is observed. On the *decreasing Re* branch, the cylinder is still in the synchronization/lock-in state and the vortex-shedding mode observed is $C(2S)$.

To highlight the effect of blockage, we now look at an Re value close to the onset of lock-in but with 1% blockage. Figure 6 shows the time histories of transverse oscillation of the cylinder and lift coefficient at Reynolds number, $Re=84.1$, for 1% blockage. The vorticity field at two time instants are also shown for both branches. From Figure 3, near the lower Re end of lock-in the *increasing* and *decreasing Re* branches are found to be virtually the same. The time histories and flow for both branches at $Re=84.1$ also show the same behavior. The response of the cylinder shows both low as well as high amplitudes of oscillation intermittently. In order to capture the intermittent behavior, the computations in the transition from initial to lower branch are computed for 1000 vortex-shedding cycles, approximately. The longest beat cycle is observed at an Re very close to the lower branch. Its period is 217 vortex-shedding cycles, approximately. All the computations for each Re in the lower branch are computed for 500 vortex-shedding cycles. From the flow pictures it is seen that it is possible to have both $2S$ and $C(2S)$ modes intermittently depending on the amplitude of oscillation of the cylinder. The low amplitude corresponds to $2S$ mode, whereas $C(2S)$ mode is observed where the amplitude of oscillation is large. It is seen that for the low blockage case, hysteresis near the lower Re end of lock-in is replaced by an intermittent behavior. The flow remains intermittent for a range of Re near the onset of

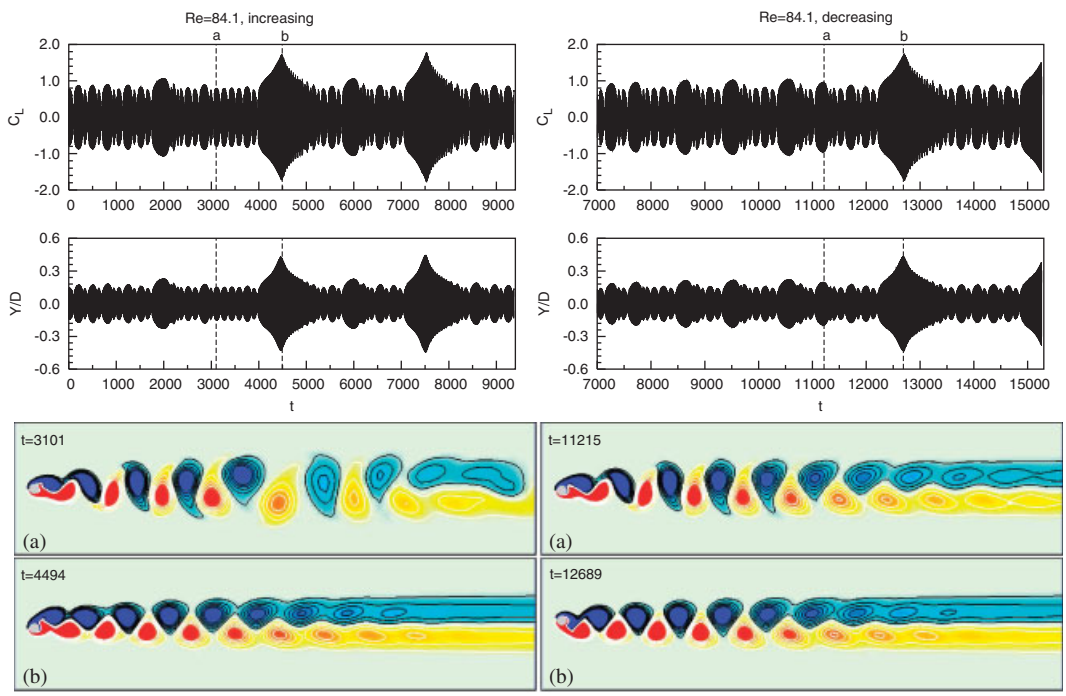

Figure 6. $Re=84.1$, $B=1\%$ flow past a freely vibrating cylinder: time histories of the lift coefficient and transverse oscillation of the cylinder for, both, increasing and decreasing branches. Also shown is the vorticity field for the unsteady flow for the two cases at two time instants.

DOI: 10.1002/fld

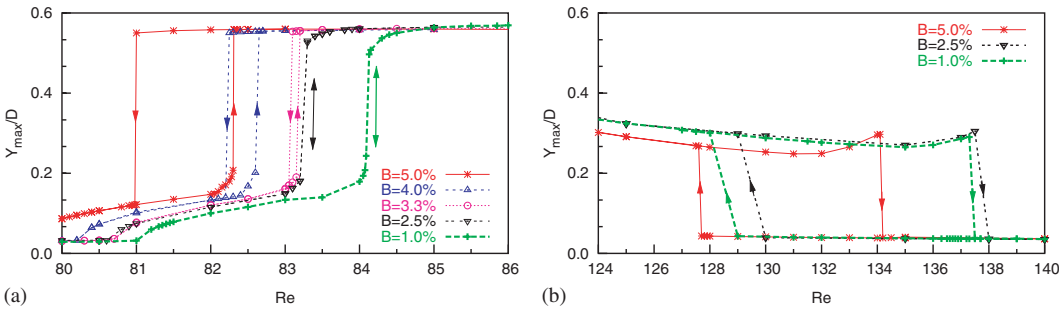

Figure 7. Variation of maximum value of transverse displacement with *Re* for different blockages near the (a) lower and (b) higher *Re* end of lock-in.

synchronization, after which only high amplitude of oscillation is observed for the *increasing Re* branch.

5.3. Effect of blockage on hysteresis

From Figures 3 and 4, it is observed that at higher blockage, the response of the cylinder and aerodynamic coefficients are hysteretic at, both, lower as well as higher *Re* ends of lock-in. However, at lower blockages, the hysteresis near the lower *Re* end of lock-in is not observed. This shows that the hysteretic behavior near the lower *Re* end depends on blockage. In order to investigate this, we look very closely at both ends of lock-in at blockages in the range 1–5%. Figure 7(a) shows the variation of the normalized maximum amplitude of the transverse oscillations for various blockages, near the lower *Re* range of the synchronization/lock-in region. It is seen that near the lower *Re* end of lock-in, the width of hysteresis loop reduces with decrease in blockage. For blockage of 2.5% and less, the hysteretic behavior completely disappears. A similar behavior is observed for in-line oscillations and aerodynamic coefficients. In general, the jump in the amplitude of cylinder response and aerodynamic coefficients occurs at a slightly smaller *Re* with increase in blockage. This is caused by the increased local acceleration of the flow as blockage increases.

The variation of the normalized amplitude of the maximum transverse oscillation at the higher *Re* end of the synchronization/lock-in region is shown in Figure 7(b). It is interesting to note that, unlike at the lower *Re* range, hysteresis at the higher *Re* end of lock-in is observed irrespective of the blockage. In fact, the hysteresis loop (in terms of ΔRe) increases with decrease in blockage at the higher *Re* end of the synchronization region. The hysteresis behavior at the higher *Re* end of synchronization has not been observed by many researchers. Recently, Klamo *et al.* [10] showed that the hysteretic jump near the higher *Re* end of lock-in is dependent on the damping.

Figure 8(a) shows the variation of the r.m.s. value of the transverse oscillations of cylinder with *Re* near the lower *Re* end of lock-in. The behavior at low blockage is found to be qualitatively different from that at high blockage. For the low blockage the increase in r.m.s. value of the response amplitude takes place in three stages: a steep jump followed by a relatively gradual change and then a sharp jump yet again. The second stage with more gradual change becomes smaller with increase in blockage and eventually disappears for $B = 3.3\%$ and higher. This suggests that

DOI: 10.1002/fld

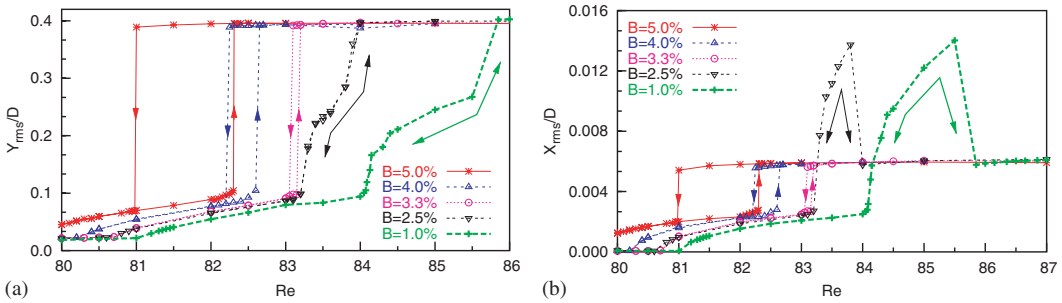

Figure 8. Variation of r.m.s. value of (a) transverse and (b) in-line displacement with *Re* for different blockages near the lower *Re* end of lock-in.

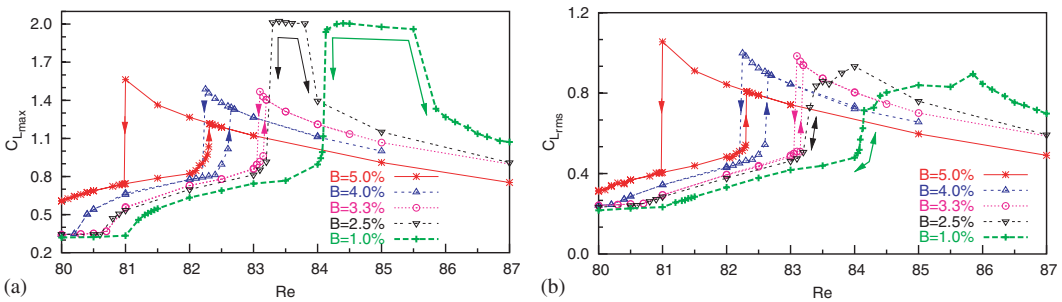

Figure 9. Variation of (a) maximum and (b) r.m.s. values of lift coefficient with *Re* for different blockages near lower *Re* end of lock-in.

the plots with r.m.s. values are significant and more meaningful in studying VIV compared with the variation of maximum values.

Figure 8(b) shows the r.m.s. value of the in-line oscillations of the cylinder near the lower *Re* end of the lock-in. Again, hysteresis is observed for $B = 3.3\%$ and higher. The variation of X_{rms} with *Re* is different for the cases with and without hysteresis. For example, the in-line response for low blockage moves to a significantly higher value before it settles to the one seen for $B = 5\%$. For the high blockage, lock-in leads to a sharp increase in in-line oscillation amplitude. However, for the low blockage the increase takes place in two stages: a steep jump followed by a relatively gradual change. The oscillation amplitude then jumps back to a lower value. The peak value of X_{rms} for the low blockage is more than twice that seen for the higher blockage.

Figure 9(a) shows the variation of the maximum amplitude of the lift coefficient for various values of blockage near the lower *Re* end of lock-in. The behavior is very similar to the one observed for X_{rms} except for one feature. For high blockage, $C_{\text{L}_{\text{max}}}$ achieves a peak value and immediately starts reducing with increase in *Re*. However, the peak value of $C_{\text{L}_{\text{max}}}$ observed for the low blockage is retained for a range of *Re* before it jumps to a lower value. This range is beyond the *Re* where the cylinder response experiences a jump. In this regime the peak amplitude of transverse oscillations increases very slowly. The range of *Re* for which the peak $C_{\text{L}_{\text{max}}}$ is retained increases with decrease in blockage. An interesting point to note is that even though the peak

DOI: 10.1002/fld

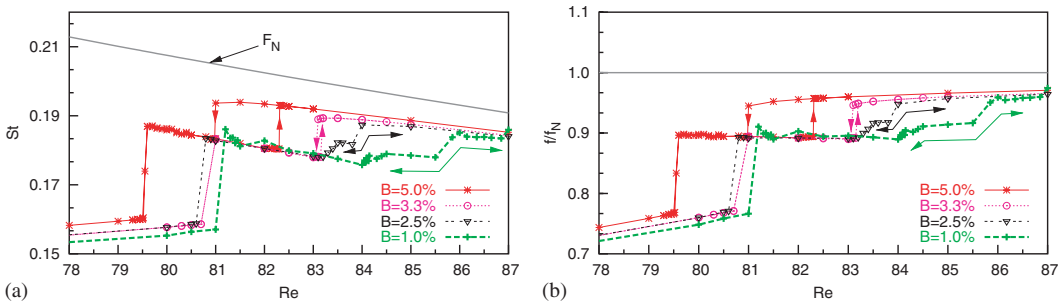

Figure 10. Variation of (a) non-dimensionalized vortex-shedding frequency and (b) frequency ratio with *Re* for different blockages near the lower *Re* end of lock-in.

$C_{L_{max}}$ is quite different for various value of blockage, the maximum amplitude of the transverse oscillations of the cylinder is same. Figure 9(b) shows the variation of r.m.s. value of the lift coefficient for various values of blockage near the low *Re* range of lock-in. Again, the hysteresis disappears for low blockage. When compared with variation of $C_{L_{max}}$, it is seen that the maximum value of $C_{L_{rms}}$ remains the same for different blockages.

Figure 10 shows the variation of Strouhal number for different values of blockages. The jump in vortex-shedding frequency occurs in two stages. The first non-hysteretic jump occurs at a value in between the vortex-shedding frequency of the stationary cylinder and the natural frequency (f_N) of the system. For all the blockages, after first jump the frequency ratio, f/f_N is $\sim$0.9. In the second stage, the jump is hysteretic at higher blockages ($B>3.3\%$). For low blockages ($B<2.5\%$), the variation is more gradual and not hysteretic in nature.

5.4. *Effect of streamwise location of boundaries*

The blockage has a very significant effect on free vibrations. What is the effect of streamwise location of computational boundaries? Do they modify the hysteretic behavior as well? To answer these questions the effect of locating the upstream and downstream boundaries is studied by carrying out computations for different values of L_u/D and L_d/D (see Figure 2). The computations are carried out close to the lower *Re* end of lock-in for a blockage of 5%. Figure 11 shows a summary of this study.

Effect of L_u: From Figure 11(a) it is observed that $L_u/D=30$ and 50 result in virtually indistinguishable results. This suggests that $L_u/D=30$ is sufficiently large to produce results for an unbounded flow. Smaller value L_u/D results in a slightly premature jump of the cylinder response from the initial to the lower branch. However, the width of the hysteresis loop is unaffected.

Effect of L_d: Figure 11(b) shows the response of the cylinder for $L_d/D=25.5$ and 50. Both sets of calculations result in virtually identical results. This study shows that the hysteretic behavior is independent of the streamwise location of the boundaries for $L_u/D>10$ and $L_d/D>25.5$.

5.5. *The phase between lift and transverse responses*

Figure 12 shows the variation of phase, ϕ, between the lift force and transverse cylinder displacement with *Re* for 5% blockage. The variation of the amplitude of cylinder vibrations is plotted alongside. The phase difference, ϕ, is computed by taking the Hilbert transform of the time histo-

DOI: 10.1002/fld

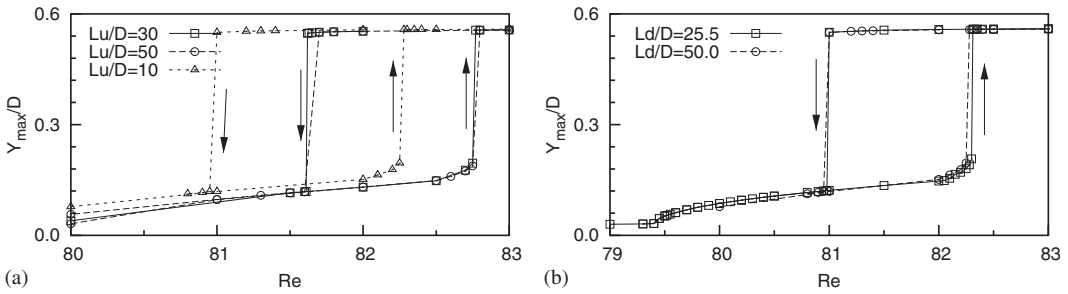

Figure 11. The effect of various boundary locations on hysteresis. (a) Effect of L_u/D, $L_d/D=50$ and $B=5\%$ (b) Effect of L_d/D, $L_u/D=10$ and $B=5\%$. The figure shows the variation of transverse displacement with Re.

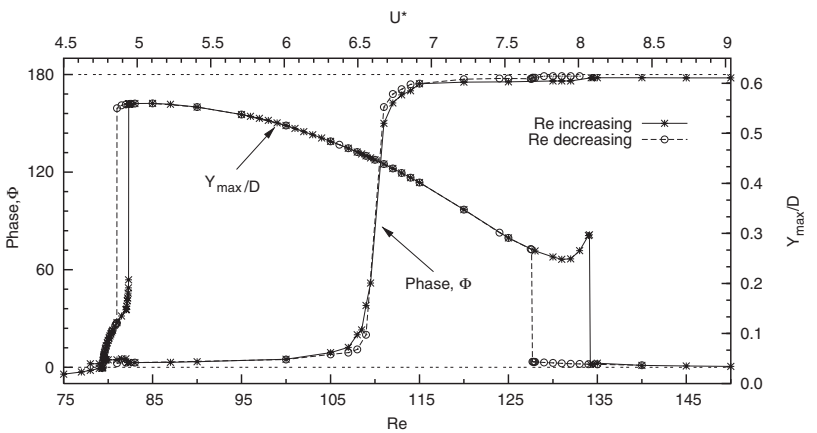

Figure 12. $B=5\%$ flow past a freely vibrating cylinder: variation of the phase, between the lift force and transverse displacement, with Re. Results for, both, the decreasing as well as increasing Re are shown. The amplitude of transverse oscillation of the cylinder is also shown for reference.

ries of the lift force and displacement for a range of Re. Details on the use of this technique can be found in the paper by Khalak and Williamson [7]. Upto $Re\sim110$ the lift is almost in phase with the transverse motion of the cylinder. A jump to $\phi\sim180°$ takes place at $Re\sim110$. Interestingly, the jump seems to take place right in the middle of the synchronization regime and it is not hysteretic in nature.

This behavior is similar to the observation of Khalak and Williamson [7] from their experiments at higher Re. They found that the jump in phase is accompanied with a shift from the upper to the lower branch of cylinder response. For low Re there is no upper branch and, therefore, in the present case the cylinder continues to remain on the lower branch. Prasanth and Mittal [25] have suggested a physical mechanism for the phase jump. By decomposing the total lift force into viscous and pressure components at various Re they found that the jump in phase is caused by the pressure component. The time-averaged flow before ($Re=90$) and after ($Re=125$) the phase jump shows interesting differences. While the $Re=125$ flow is quite similar to the mean flow past

DOI: 10.1002/fld

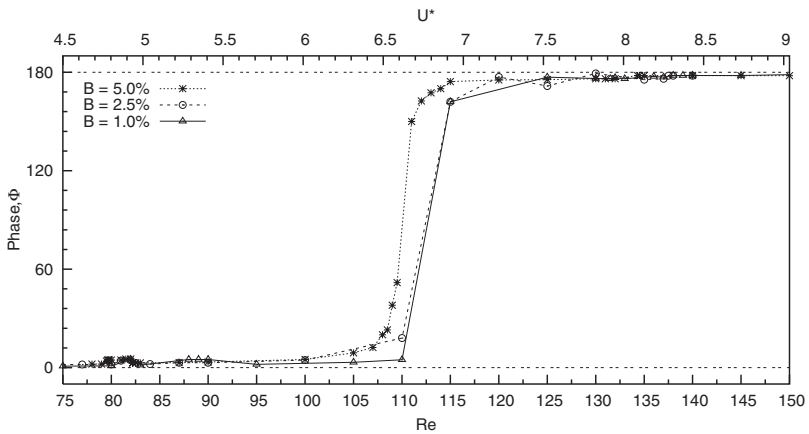

Figure 13. The variation of phase, between lift force and transverse displacement, with *Re* for different values of blockage.

a stationary cylinder, the $Re=90$ flow shows a pair of counter rotating vortices in the near wake. Figure 13 shows the variation of the phase with *Re* for various blockages. It is found that the behavior is fairly independent of the blockage. A close analysis of Figures 4 and 12 shows that the jump in phase occurs at a Reynolds number where the vortex-shedding frequency becomes exactly equal to the natural frequency of the system.

6. CONCLUSIONS

Incompressible flow past a freely oscillating circular cylinder of low non-dimensional mass ($m^*=10$) has been investigated in the two-dimensional laminar flow regime ($60<Re<150$) using a stabilized finite element method. With 5% blockage, the response of the cylinder is hysteretic at lower as well as higher *Re* ends of the synchronization region. The hysteresis loop at the higher *Re* end of synchronization is almost five times larger than the one at the lower *Re* end. It is found that the hysteresis loop at the lower *Re* end of synchronization region becomes smaller with decrease in blockage, before getting completely eliminated for a blockage of 2.5% and less. The hysteresis at the higher *Re* end of synchronization region is found to exist for all values of blockage. In fact, unlike at the lower *Re* end of lock-in, the hysteresis loop width at the the higher *Re* end of synchronization is found to increase with decrease in blockage. Even though the amplitude of the cylinder response is virtually the same at all blockages, the maximum lift coefficient is observed to be much higher in the low blockage case. The behavior of in-line displacement and vortex-shedding frequency is also different for low and high blockages. This indicates that the flows at high and low blockage cases are indeed qualitatively different. It is shown that the variation of r.m.s. values of the aerodynamic quantities with *Re* is less affected by blockage compared with the variation of maximum values. A study of the effect of various domains on the response of the cylinder shows that the upstream distance ($L_u>10D$) and downstream distance ($L_d>25.5D$) from the center of the cylinder do not have a significant influence on the response of the cylinder and on hysteresis. The hysteresis loop width is virtually the same in all the cases. This underlines the significance

DOI: 10.1002/fld

of blockage in VIV studies. These results have been obtained at low *Re* in the laminar regime. While the conclusions are not necessarily valid at higher *Re*, this effort sets up a case for the need of a detailed study of blockage effect at higher *Re* as well. The phase angle, ϕ, between lift force and transverse displacement of the cylinder shows a 180° jump approximately at the middle of the synchronization region. This jump in phase is not hysteretic in nature and is observed at low as well as high blockages.

REFERENCES

1. Williamson CHK, Govardhan R. Vortex induced vibration. *Annual Review of Fluid Mechanics* 2004; **36**:413–455.
2. Bearman PW. Vortex shedding from oscillating bluff bodies. *Annual Review of Fluid Mechanics* 1984; **16**:195–222.
3. Sarpkaya T. Vortex-induced oscillations—a selective review. *Journal of Applied Mechanics* 1979; **46**:241–258.
4. Sarpkaya T. A critical review of the intrinsic nature of vortex-induced vibrations. *Journal of Fluids and Structures* 2004; **19**:389–447.
5. Feng CC. The measurement of vortex-induced effects in flow past a stationary and oscillating circular cylinder and d-section cylinders. *Master's Thesis*, University of British Columbia, 1968.
6. Bishop RED, Hassan AY. The lift and drag forces on a circular cylinder oscillating in a flowing fluid. *Proceedings of the Royal Society of London*, *Series A* 1964; **277**:51–75.
7. Khalak A, Williamson CHK. Motion, forces and mode transitions in vortex-induced vibrations at low mass damping. *Journal of Fluids and Structures* 1999; **13**:813–851.
8. Brika D, Laneville A. Vortex induced vibrations of long flexible circular cylinder. *Journal of Fluid Mechanics* 1993; **250**:481–508.
9. Singh SP, Mittal S. Vortex-induced oscillations at low Reynolds numbers: hysteresis and vortex shedding modes. *Journal of Fluids and Structures* 2005; **20**:1085–1104.
10. Klamo JT, Leonard A, Roshko A. The effects of damping on the amplitude and frequency response of a freely vibrating cylinder in cross-flow. *Journal of Fluids and Structures* 2006; **22**:845–856.
11. Williamson CHK, Roshko A. Vortex formation in the wake of an oscillating cylinder. *Journal of Fluids and Structures* 1988; **2**:355–381.
12. Ongoren A, Rockwell D. Flow structure from an oscillating cylinder. Part 1. Mechanisms of phase shift and recovery in the near wake. *Journal of Fluid Mechanics* 1988; **191**:197–223.
13. Ongoren A, Rockwell D. Flow structure from an oscillating cylinder. Part 2. Mode competition in the near wake. *Journal of Fluid Mechanics* 1988; **191**:225–245.
14. Govardhan R, Williamson CHK. Modes of vortex formation and frequency response of a freely vibrating cylinder. *Journal of Fluid Mechanics* 2000; **420**:85–129.
15. Prasanth TK, Behara S, Singh SP, Kumar R, Mittal S. Effect of blockage on vortex-induced vibrations at low Reynolds numbers. *Journal of Fluids and Structures* 2006; **22**:865–876.
16. Carberry J, Sheridan J, Rockwell D. Controlled oscillations of a cylinder: forces and wake modes. *Journal of Fluid Mechanics* 2005; **538**:31–69.
17. Norberg C. Fluctuating lift on a circular cylinder: review and new measurement. *Journal of Fluids and Structures* 2003; **17**:57–96.
18. Mittal S, Tezduyar TE. A finite element study of incompressible flows past a oscillating cylinders and airfoils. *International Journal for Numerical Methods in Fluids* 1992; **15**:1073–1118.
19. Stansby PK. The locking-on of vortex shedding due to the cross-stream vibration of circular cylinders in uniform and shear flows. *Journal of Fluid Mechanics* 1976; **74**:641–665.
20. Tezduyar TE, Behr M, Liou J. A new strategy for finite element computations involving moving boundaries and interfaces—the deforming-spatial-domain/space–time procedure. I: the concept and the preliminary tests. *Computer Methods in Applied Mechanics and Engineering* 1992; **94**(3):339–351.
21. Tezduyar TE, Behr M, Mittal S, Liou J. A new strategy for finite element computations involving moving boundaries and interfaces—the deforming-spatial-domain/space–time procedure. II: computations of free-surface flows, two liquid flows and flows with drifting cylinders. *Computer Methods in Applied Mechanics and Engineering* 1992; **94**(3):353–371.
22. Tezduyar TE, Mittal S, Ray SE, Shih R. Incompressible flow computations with stabilized bilinear and linear equal-order-interpolation velocity pressure elements. *Computer Methods in Applied Mechanics and Engineering* 1992; **95**:221–242.

DOI: 10.1002/fld

23. Mittal S, Kumar V. Finite element study of vortex-induced cross-flow and in-line oscillations of a circular cylinder at low Reynolds numbers. *International Journal of Numerical Methods in Fluids* 1999; **31**:1087–1120.
24. Mittal S, Kumar V. Flow induced oscillations of two cylinders in tandem and staggered arrangement. *Journal of Fluids and Structures* 2001; **15**:717–736.
25. Prasanth TK, Mittal S. Vortex-induced vibrations of a circular cylinder at low Reynolds numbers. *Journal of Fluid Mechanics* 2008; **594**:463–491.

DOI: 10.1002/fld